International Journal of Environmental Sciences
ISSN: 2229-7359
Vol. 11 No. 21s, 2025
https://www.theaspd.com/ijes.php

Insight into Structural, Spectral and Biological Description of Aluminium Nitrate Glutaric Acid: DFT Approach

Reshma J. S[1], Joselin Beaula T[2]*. R. S. Bemina[3], S. R. Gibin[4]
[1]Research Scholar, Reg.No: 22213082132011, Department of Physics and Research Centre, Malankara Catholic College, Mariagiri-629153, Affiliated to Manonmaniam Sundaranar University, Abishekapatti-627012, Tirunelveli, Tamilnadu, India.
[2]Assistant Professor, Department of Physics and Research Centre, Malankara Catholic College, Mariagiri-629153, Tamilnadu, India.
[3]Department of Physics and Research Centre, Malankara Catholic College, Mariagiri-629153, Tamilnadu, India
[4] Associate Professor of Physics, Sree Sakthi Engineering College (Autonomous), Karamadai, Coimbatore-641104, Tamil Nadu, India (Affiliated to Anna University, Chennai).
*joselinbeaula@gmail.com

Abstract
*The synthesis of aluminum nitrate glutaric acid was confirmed by PXRD, and the optimized structure of the compound was compared with DFT calculations at the B3LYP/6-311++G** level basis set to achieve complete assignments. Vibrational analyses were conducted using infrared and Raman spectra, and the charge transfer ionic interaction strategy was studied using the TD-DFT method to identify the electronic transition exhibited in the UV–visible spectrum. The electron localization function (ELF) and analysis provide new insight into the chemical bonding of MP. The chemical interactions within the molecule were investigated through NCI and IRI investigations.*

1. INTRODUCTION

Since antibacterial resistance affects the global economy, it is considered one of the most important public health concerns. Antibiotic resistance is reducing the number of viable treatment options while raising the morbidity and death rate of bacterially caused infectious diseases. Metallic complex compounds that still have more effective biological properties continue to be investigated in the literature. Therefore, Aluminium complex was synthesized and characterized in this study. Aluminium nitrate is a versatile inorganic salt with a wide range of industrial, laboratory, and environmental applications. Aluminium nitrate has some intriguing biological and biomedical applications, especially when used as a component in advanced materials. Glutaric acid is a versatile compound with a wide range of industrial and biochemical applications. - Serves as an intermediate in the production of antidepressants, anti-inflammatory drugs, and other pharmaceutical agents [1] - Glutaric acid is used in template synthesis to create metal-based macrocyclic compounds with potential antibacterial and antifungal properties[2]. It serves as a building block in synthesizing drugs and surfactants [3].

In this study, present the synthesis, crystallographic structure and physical properties of Aluminium Nitrate Glutaric Acid (ANGA). Title compound was characterized using single crystal X-ray diffraction (XRD), FT-IR, Raman and UV-vis spectroscopic methods. In order to examine the physical and chemical properties of molecules, DFT shows good performance on vibrational frequencies and geometries of compounds. Furthermore, the interaction of the molecule will be determined. Therefore, this study is expected to provide both theoretical and experimental information in the design and production of new antibacterial drugs.

2. Experimental Details

2.1 Material Synthesis and crystal growth

Ethanol and water were used as a combined solvent to manufacture the precursor ingredients of glutaric acid (Moly chem) and aluminum nitrate (Spectrum Chemical) in order to achieve solution growth. At room

temperature, a suitable amount of aluminum nitrate was first dissolved in ethanol. Following the full dissolution of the aluminum nitrate, a tiny amount of water solvent was added gradually to the aluminum nitrate solution in order to introduce the acid complex glutaric acid. After that, the entire solution was continuously stirred for six hours in order to achieve saturation. Whatman filter paper with pore sizes of around 100 mm was used to filter the saturated solution. In order to accomplish the nucleation process and supersaturation, the resulting solution is lastly permitted to delay evaporation. An optical crystal of high grade was extracted from the mother solution. To enhance the quality of the crystal by increasing the compound's purity, the resulting crystal is put through the recrystallization process two or three times. A high-quality crystal was collected following the 35-day growing phase.

2.2 Characterization techniques

The FT-IR spectrum of ANGA was recorded on a Perkin Elmer FT-IR 8000 spectrophotometer in the range of 4000–400 cm^{-1} using the KBr pellet technique at room temperature. A FT-Raman spectrum has been recorded on a Bruker RFS 27: Standalone FTRaman Spectrometer with a Nd: YAG laser source at 1064 nm and a resolution of 2 cm^{-1} in the region 4000–50 cm^{-1}. The electronic absorption spectrum was measured in methanol using a JASCO UV–Vis spectrophotometer in the range of 200–800 nm.

3. Computational analysis

With the support of the Gaussian'09w software package [4], DFT computations were executed using the B3LYP functional method with the basis set of 6-311++g(d,p) for the complex DAZM structure. The theoretical UV-Vis spectrum was simulated using the Time Dependent-Density Functional (TD-DFT) methodology with the DMSO as a solvent. Charge transfer excitation and Density of states analysis (DOS) were performed using GaussSum[5]. Multiwfn [6] executes the NCI, DORI and IRI analyses, and their isosurface mapping and scatter graphs were visualized using the VMD (Visual Molecular Dynamics) program [7].

4. RESULTS AND DISCUSSION

4.1 PXRD Analysis

The XPert PRO powder X-ray diffractrometer was used to analyze the powdered sample of the generated crystal by powder X-ray diffraction. The single crystal X-ray diffraction data complements the data from the powder X-ray diffraction investigation. Figure 1 displays the indexed powder X-ray diffraction pattern. From this, the crystallinity, phase purity, and structural characteristics of solid materials are confirmed using PXRD of ANGA.

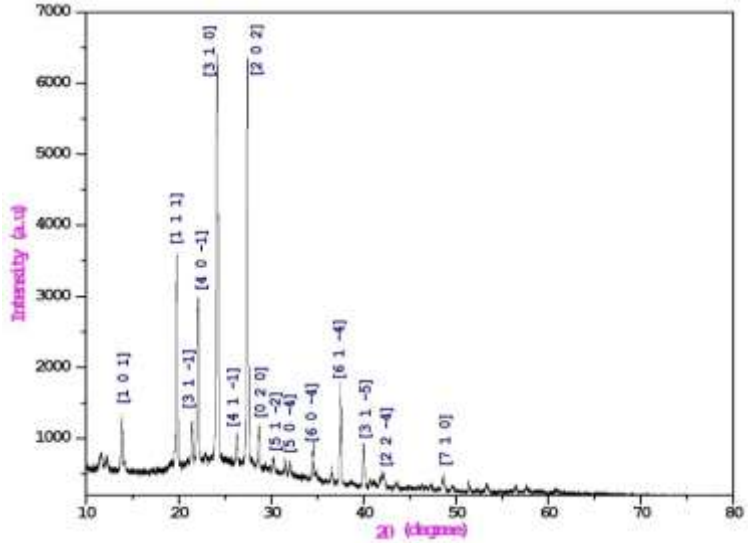

Fig. 1 Indexed powder XRD pattern of ANGA

4.2 Structural Analysis

Table 1 provided optimized geometrical parameters, including bond lengths, and Valance angles. Protonated groups that are not engaged in binding are suggested by O-H lengths of about 0.969 Å. Longer N–O bonds (>1.3 Å) indicate interaction with Al^{3+}, which is compatible with partial electron sharing or ligand displacement. A potential van der Waals or through-space contact indicated by the bond length of O11–O15 is 3.005 Å. Tetrahedral carbon centers often have valence angles of 111.32° in organic segments (such as C19–C18–C20 = 111.32°). The C–H–C and H–C–H angles are in the range of 109° to 111°, which is in line with sp^3 hybridization. Planarity and charge distribution are impacted by delocalization and lone-pair repulsion, which are reflected in N-O-C angles that range from 153° to 169°. Tight and diverse coordination angles, long hydrogen bonding networks, and strained internal angles inside the aluminum coordination sphere all support the idea that the ANGA molecule is producing a supramolecular assembly or metal–organic aerogel. Intermolecular hydrogen bonding contact is made easier by the O11...H30-O15 (2.8 Å) bond distance, which is much shorter than van der Waals separation (3 Å), allowing molecules with better biological profiles to be constructed. [8]

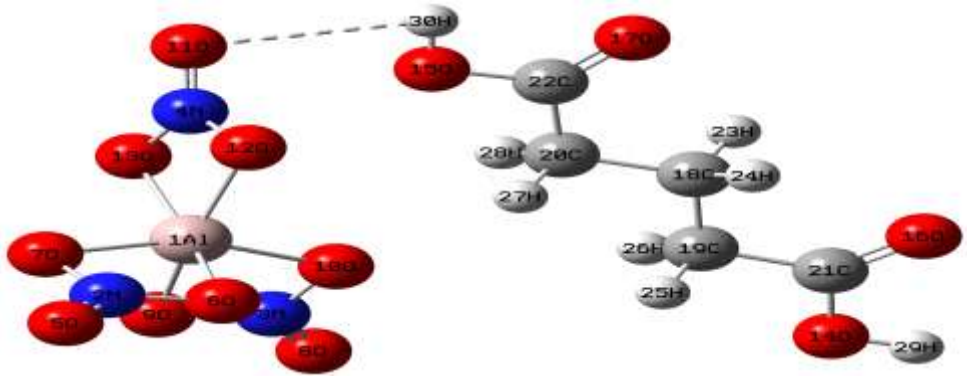

Fig. 2 Optimized Structure of ANGA

Table 1 optimized geometrical parameters of ANGA

Bond length	Calculated	Valance angle	Calculated	Valance angle	Calculated
Al1-O6	1.928	O6- Al 1-O7	67.39	C21-O14-H29	107.16
Al 1-O7	1.930	O6- Al 1-O9	99.66	N4-O15-C22	153.11
Al 1-O9	1.934	O6- Al 1-O10	97.48	O11-O15-C22	169.60
Al 1-O10	1.932	O6- Al 1-O12	98.43	C22-O15-H30	107.01
Al 1-O12	1.927	O6- Al 1-O13	158.57	C19-C18-C20	111.32
Al 1-O13	1.926	O7- Al 1-O9	97.80	C19-C18-H23	109.97
N2-O5	1.182	O7- Al 1-O10	157.37	C19-C18-H24	109.82
N2-O6	1.305	O7- Al 1-O12	99.83	C20-C18-H23	109.96
N2-O7	1.304	O7- Al 1-O13	98.17	C20-C18-H24	109.85
N3-O8	1.183	O9- Al 1-O10	67.18	H23-C18-H24	105.75
N3-O9	1.301	O9- Al 1-O12	158.48	C18-C19-C21	113.36
N3-O10	1.305	O9- Al 1-O13	97.91	C18-C19-H25	111.47
N4-O11	1.182	O10- Al 1-O12	98.98	C18-C19-H26	111.48
N4-O12	1.303	O10- Al 1-O13	100.56	C21-C19-H25	107.34
N4-O13	1.303	O12- Al 1-O13	67.46	C21-C19-H26	107.36
N4-O15	3.104	O5-N2-O6	124.84	H25-C19-H26	105.36
N4-H30	3.258	O5-N2-O7	124.89	C18-C20-C22	113.41
O10-H27	2.622	O6-N2-O7	110.25	C18-C20-H27	111.66
O11-O15	3.005	O8-N3-O9	124.96	C18-C20-H28	111.23
O11-H30	2.833	O8-N3-O10	124.67	C22-C20-H27	107.71

O14-C21	1.358	O9-N3-O10	110.35	C22-C20-H28	106.93
O14-H29	0.969	O11-N4-O12	124.78	H27-C20-H28	105.43
O15-C22	1.363	O11-N4-O13	124.87	O14-C21-O16	122.43
O15-H30	0.969	O12-N4-O13	110.33	O16-C21-C19	111.20
O16-C21	1.204	O12-N4-O15	93.67	O15-22-O17	126.35
O17-C22	1.203	O12-N4-30	96.19	O15-C22-C20	122.04
C18-C19	1.528	O13-N4-O15	104.75	O17-C22-C20	111.32
C18-C20	1.528	O13-N4-30	119.29		
C18-H23	1.091	Al 1-O6-N2	91.20		
C18-H24	1.092	Al 1-O7-N2	91.15		
C19-C21	1.510	Al 1-O9-N3	91.25		
C19-H25	1.096	Al 1-O10-N3	91.20		
C19-H26	1.096	Al 1-O10-H27	136.26		
C20-C22	1.509	N3-O10-H27	119.46		
C20-H27	1.094	Al 1-O12-N4	91.08		
C20-H28	1.097	Al 1-O13-N4	91.11		

4.3 Optical properties

4.3.1 HOMO LUMO and DOS Analysis

The energy values of LUMO, HOMO, and energy gap provide crucial information for determining a molecule's optical characteristics, chemical stability, and molecular electrical transport characteristics. The title compound's lowest unoccupied molecular orbital (LUMO) and highest occupied molecular orbital (HOMO) energy values were calculated. Fig. 6 displays the relevant molecular orbital HOMO and LUMO DOS plots for ANGA. The charge transfer of ANGA was confirmed by the presence of HOMO nodes on the glutaric acid and LUMO nodes on the aluminum nitrate. The title molecule's HOMO and LUMO energies were determined to be -3.75978 eV and -8.04013 eV, respectively. The lowest energy gap between HOMO and LUMO, which was calculated to be 4.2804 eV, validates the bioactivity.

The number of states in a unit energy interval is displayed by the density of states (DOS). Fig. S3 shows the complex's DOS analysis curve. The state distribution of molecular systems can be inferred from DOS. According to this analysis, occupied orbitals with energies between -20 and 0 eV have the highest density of states. Furthermore, optical transition probabilities depend on it. The complex's DOS analysis was computed in the gas phase for this investigation.

HOMO LUMO and DOS Analysis

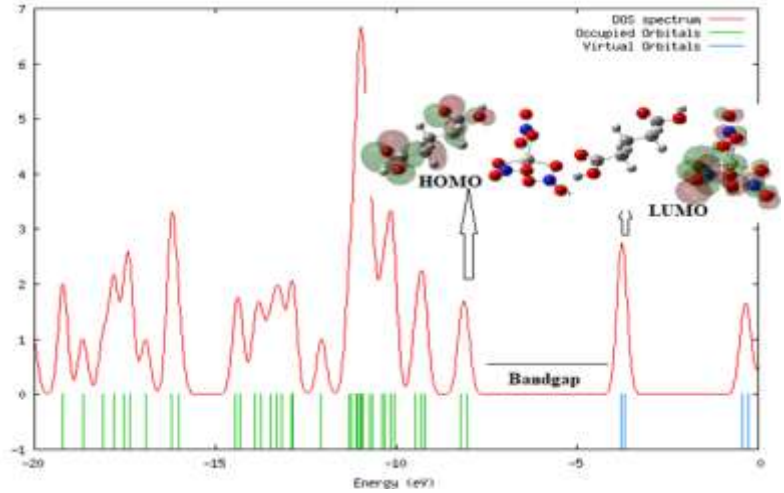

4.3.2 UV - vis spectral Analysis

In Fig. 3, the optical behaviour of ANGA was investigated, and the UV-vis absorption spectrum experimental and theoretical of ANGA were given. In the title compound's UV-vis spectrum, strong absorption bands were seen, with their centers at 314.5 nm, 311 nm, and 307 nm. These absorption bands have respective band gap energies of 3.94, 3.98, and 4.03 eV. The Table 2 presents theoretical values that exhibit agreement with both experimental and HOMO LUMO band gap values. The $\pi \rightarrow \pi^*$ transition in the organic cation is responsible for the examined absorption peaks. The table shows theoretical bands with significant contributions from HOMO→LUMO, where the shift between calculated and experimental energies is primarily ascribed to hydrogen bonding interactions.

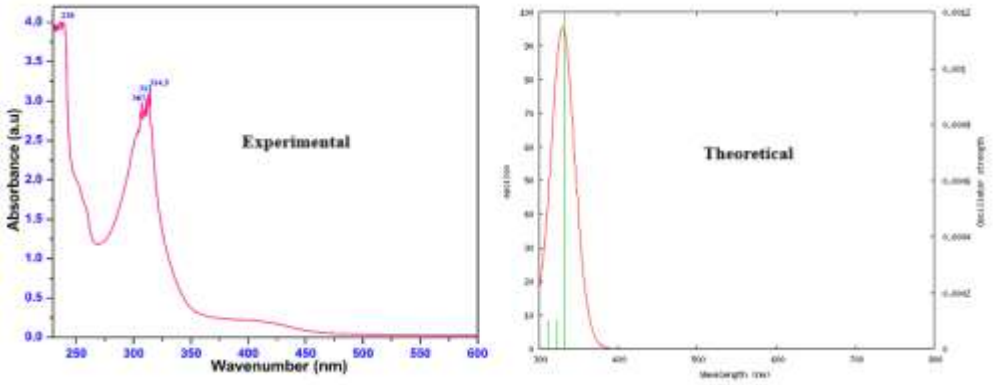

.

Fig. 3 UV - vis Spectra of ANGA

Table 2 UV-visible wavelength and their contributions

Energy (cm^{-1})	Theoretical		Experimental		Major contributions
	Wave length (nm)	Band gap eV	Wave length (nm)	Band gap eV	
30209	331	3.7462			H-1→LUMO (21%), HOMO→LUMO (39%), HOMO→L+1 (23%)
30984	322	3.8509	314.5	3.9428	HOMO→LUMO (10%), HOMO→L+1 (60%), HOMO→L+2 (20%)
32066	311	3.9871	311.0	3.9871	H-1→L+1 (64%), HOMO→LUMO (21%), HOMO→L+2 (10%)
32222	310	4.0000			H-1→L+1 (15%), H-1→L+2 (20%), HOMO→LUMO (21%), HOMO→L+1 (12%), HOMO→L+2 (32%)
32598	306	4.0523	307.0	4.0391	H-1→LUMO (61%), HOMO→L+2 (23%), HOMO→L+2 (11%), H-1->L+1 (8%)

H →HOMO; L →LUMO

4.4 Spectral Analysis

The ANGA has been subjected to vibrational spectral analysis using Raman and FT-IR spectra. A thorough discussion and identification of the fundamental modes linked to the chemical ANGA were conducted. ANGA's FT-IR and Raman spectra are displayed in Figures 3 and 4, and Table 3 lists the FT-IR and FT-Raman wave numbers along with their corresponding assignments.

4.4.1 Carboxylic acid vibrations

A high peak around 1686 cm^{-1} in IR and 1652 cm^{-1} in Raman due to C=O stretching confirms the presence of a free carboxylic acid in ANGA because the production of molecular adduct does not entail any proton transfer. A broad band at 3379 and 3255 cm^{-1} in Raman shows the O-H stretching, and the redshift of this

band indicates the strength of the intermolecular O-H...O hydrogen bonding effect [9]. The cause of absorption at 1418 cm^{-1} is in-plane bending of C-O-H.

4.4.2 CH_2 group vibrations

While symmetric stretching modes, which are projected to be in the range 2950 ±45 cm^{-1}, are seen as a strong band at 2952, 2893 cm^{-1} in IR and 2951, 2917 cm^{-1} in Raman, asymmetric CH_2 stretching modes, which are predicted to be in the range 3000±45 cm^{-1}[10-12] are seen at 3039 cm^{-1} in IR and 2978 cm^{-1} in Raman. The strong band at 1467 cm-1 in infrared and 1459 cm-1 in Raman is thought to be the CH_2 scissoring mode, which is thought to be in the 1445±35 cm-1 area. The estimated range for CH_2 twisting and wagging modes is 1350–1150 cm^{-1} [10-12]. CH_2 wagging is shown in IR at 1203, 1165, and in Raman at 1162, while CH2 twisting is seen in IR at 1301, 1406 cm^{-1}, and 1297 cm^{-1} in Raman.

4.4.3 Al-O and Skeletal vibration

For different types of aluminum oxide, the Al-O stretching vibration area in Infrared (IR) spectroscopy usually lies between 500 and 1000 cm^{-1} [13]. It may be seen in IR at 664 cm^{-1}, 760 cm^{-1}, and 911 cm^{-1}, as well as in Raman at 890 cm^{-1}, 772 cm^{-1}, and 678 cm^{-1}. It is challenging to determine the C-C stretching wavenumbers in the side chains because it can be challenging to distinguish them from other vibrations. At 1441 cm^{-1}, C–C stretching vibrations that were predicted to occur in the 1400–1600 cm^{-1} region [14] are detected.

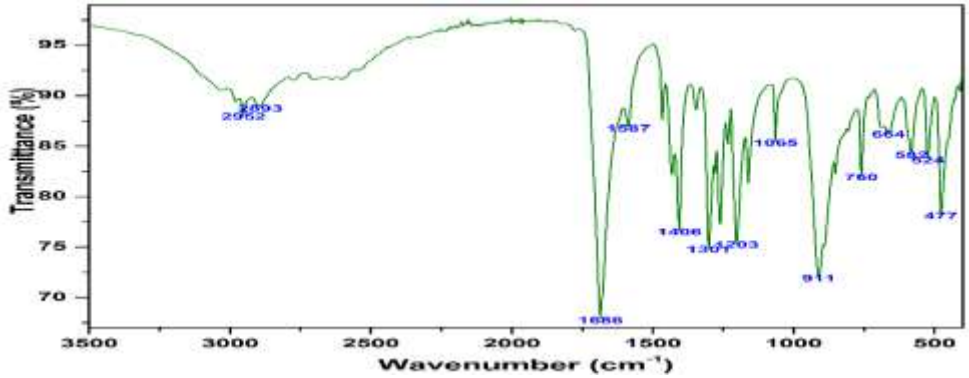

Fig. 3 FT IR spectrum of ANGA

Table 3 Vibrational Assignments of ANGA

IR	Raman	Assignments	IR	Raman	Assignments
	3379	O-H stretching	1226		CH2 twisting
	3255	O-H stretching	1203		CH2 wagging
	3113	C-H stretching	1165	1162	CH2 wagging
3039		Asymmetric CH2 stretching	1065	1063	C-O –H bending
	2978	Asymmetric CH2 stretching		940	CH2 bending
2952	2951	Symmetric CH2 stretching	911		Al-O stretching
	2917	Symmetric CH2 stretching		890	Al-O stretching
2893		Symmetric CH2 stretching	760	772	Al-O stretching
1686		C=O stretching	664	678	Al-O stretching
	1652	C=O stretching	582		C-H torsion
1587		C –C stretching	524		O-H torsion
	1441	C –C stretching	477		Al-O torsion
1467	1459	CH2 scissoring		444	Al-O torsion
	1418	C-O-H in-plane bending		319	Al-O torsion
1406		CH2 scissoring		87	Al-O torsion
1301	1297	CH2 twisting		72	O-H torsion

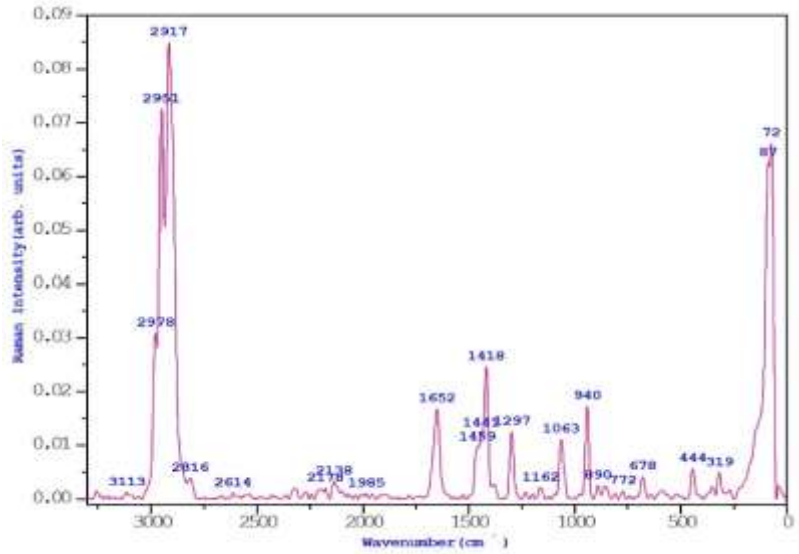

Fig.4 Raman spectrum of ANGA

4.5 Topological Analysis.

4.5.1 Electrostatic potential

The distribution of electric charge across a compound's molecular surface is known as its electrostatic potential, and it affects how the compound interacts with other molecules, particularly in chemical or biological systems and this map is given in Fig 5. Based on their chemical makeup, we can deduce some general properties for a combination such as aluminum nitrate–glutaric acid. Nitrate ions (NO_3^-) are delocalized and contribute to overall polarity, while blue zones surrounding aluminum ions (Al^{3+}) have a strong positive charge. Aluminum nitrate is a highly ionic compound. The red areas surrounding dicarboxylic acid contain two acidic groups that can donate protons and create hydrogen. Regions of high polarity would be present throughout the molecule, particularly in the vicinity of the Al^{3+} and COO^- groups. A concentrated positive potential is contributed by the aluminum ion. Negative regions are contributed by the carboxylate and nitrate groups. Thus, it creates powerful hydrogen and ionic bonds with polar or negatively charged molecules. It may also interact with bacterial membranes or proteins, which could account for its antibacterial properties.

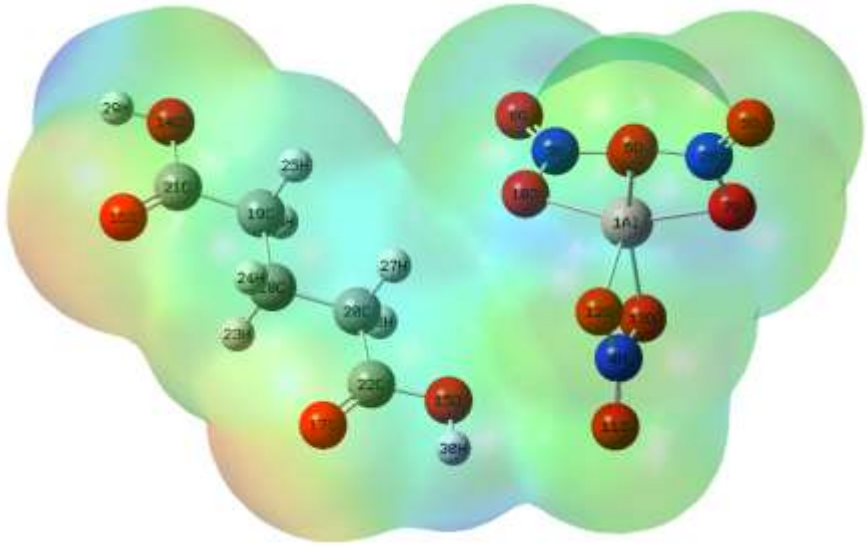

Fig. 5 Electrostatic potential of ANGA

4.5.2 ELF and LOL Analysis

To see and measure electron localization in molecules, quantum chemists employ the Electron Localization Function (ELF) and the Localized Orbital Locator (LOL) and these plots are given in Fig. 6. To comprehend molecule stability and reactivity, these investigations aid in locating delocalized electrons, lone pairs, and covalent bonding areas. According to its electropositive character, ELF would probably exhibit low electron localization around the aluminium core. LOL may emphasize the directed bonding between aluminium and oxygen atoms from glutaric acid's carboxyl and nitrate groups. A Neighbouring oxygen atoms with high ELF values are lone pairs. Covalent C=O bonds would show up on LOL and ELF maps as localized areas. ELF values would be modest for delocalized π-electrons throughout the NO_3^- group. LOL could show where the atoms of nitrogen and oxygen intersect in orbit. Glutaric acid and nitrate group hydrogen bonds can be seen intramolecularly or intermolecularly using ELF and LOL. Reactivity sites for electrophilic and nucleophilic assault and the realization of metal-ligand interactions in coordination complexes are derived from ELF and LOL. It validates electron delocalization and stability, which affect solubility and biological activity.

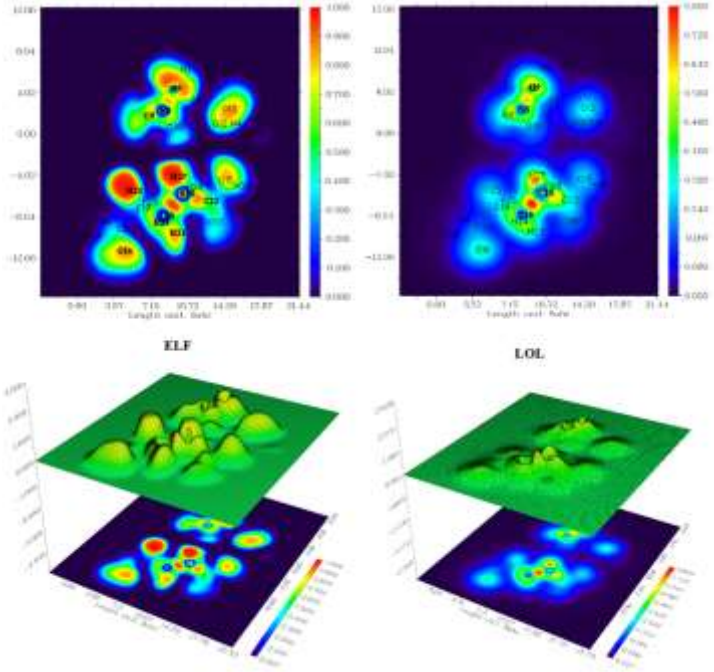

Fig. 6 ELF and LOL plot of ANGA

4.5.3 DORI Analysis

The quantum chemistry descriptor described as the Density Overlap Region Indicator, or DORI, is used to visualize and examine both covalent and non-covalent interactions in molecules [15] and this plot is given in Fig.7. Finding areas where atoms share or clash with electron density is made easier by this scalar field, which is derived from electron density and its derivatives. Glutaric acid's dicarboxylic acid can function as a bidentate ligand and form chelates with metal ions, while aluminum nitrate supplies $Al2^+$ ions that can coordinate with ligands. Al^{3+} and the carboxylate groups may have metal ligand bonding regions, according to DORI analysis. Van der Waals forces and hydrogen bonds are examples of non-covalent interactions that occur within the complex. overlap in electron densities that reveals the type and degree of coordination. When fluxional molecules are analyzed using DORI, covalent and non-covalent interactions in dynamic systems can be revealed.

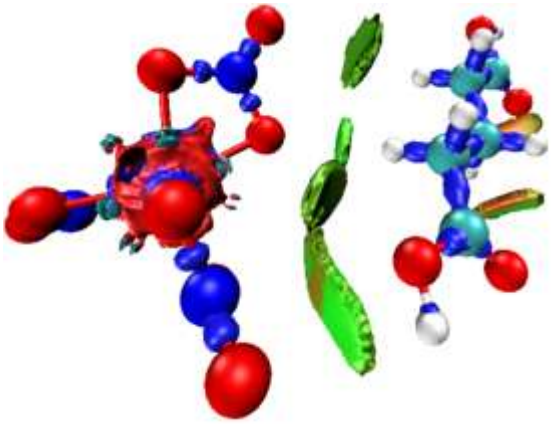

Fig. 7 DORI plot of ANGA

4.5.4 RDG analysis of ANGA

RDG scatter plots and isosurface visualizations are highly effective methods for examining the non-covalent interactions and bonding properties in an aluminum nitrate glutaric acid system and RDG plot of ANGA is given in Fig.8. X-axis indicates the nature of interaction, positive values indicate repulsive interactions like steric clashes, while negative values indicate attractive interactions like hydrogen bonding and van der Waals. Areas of low electron density gradient, characteristic of non-covalent interactions, are highlighted on the Y-axis. RDG analysis highlights hydrogen bonds between nitrate and glutaric acid, identifies van der Waals contacts in the molecular framework, and reveals metal ligand coordination zones between Al^{3+} and carboxylate groups. Strong attractive interactions are represented by blue in RDG isosurfaces, weak van der Waals interactions by green, and steric repulsion by red. Perspectives for ANGA illustrates how the carboxylate groups of glutaric acid chelate Al^{3+}. maps packing interactions and intramolecular hydrogen bonds, aids in the differentiation of non-covalent stabilization from ionic bonding.

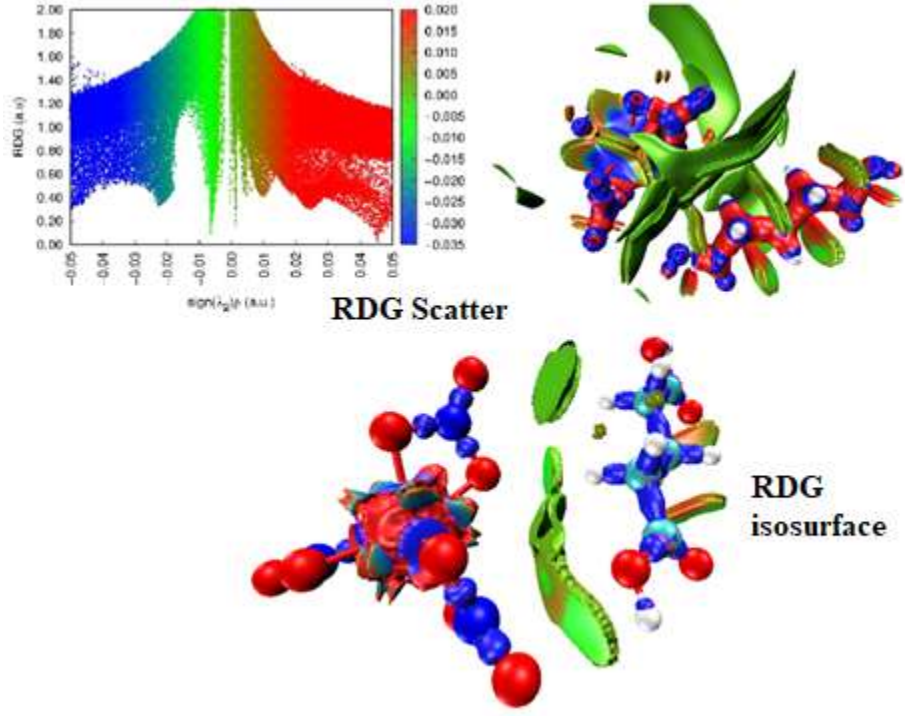

Fig. 8 RDG plot of ANGA

4.6 Antibacterial Activity Analysis

The antibacterial activity results of the target compounds are shown in Table 4, and a visual depiction is given in Figure 9. At a concentration of 0.2, the antimicrobial agent shows increased activity, leading to larger inhibition zones in the majority of organisms. E. coli and B. cereus have much larger inhibition zones, indicating that they are more active than other microorganisms. The zone of inhibition grew dramatically from 0.1% to 0.2% for all bacteria except Staphylococcus aureus, indicating a dose-dependent antibacterial action of aluminum nitrate-glutaric acid that confirms higher concentrations increase efficacy. In comparison to the antibiotic control, Staphylococcus aureus exhibited a negligible response of 0.2% (6 mm), suggesting limited susceptibility to the tested compound. Cefpodoxime, the positive control, was very effective against Staphylococcus aureus (22 mm) when compared to controls; however, none of the other strains responded, suggesting potential resistance. As anticipated, the Negative Control revealed no inhibition (R) for any strain.

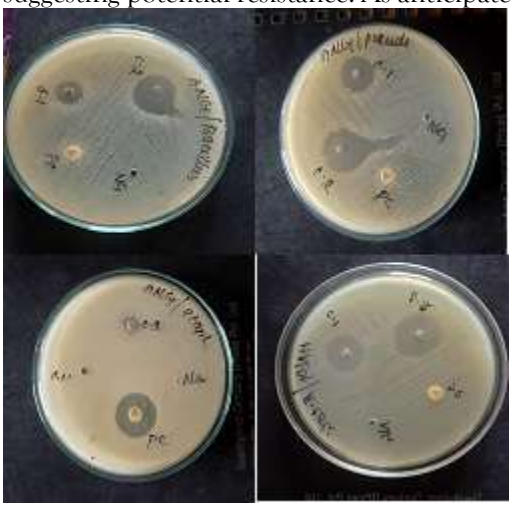

Fig. 9 Antibacterial Activity

Table 4 Antibacterial Activity

Microorganisms	Zone of Inhibition (diameter in mm)			
	Concentration		Positive Control	Negative Control
	0.1	0.2		
Escherichia coli	10	20	R	R
Pseudomonas auroginosa	12	20	R	R
Bacillus cereus	9	19	R	R
Staphylococcus aureus	R	6	22	R
(PC-Positive Control- Cefpodoxime) NG-Negative Control				

CONCLUSION

Slow evaporation was used to grow AGNA from an aqueous solution. The current study used a quantum chemical computation approach to investigate the effects of hydrogen bonding interactions on the structural, vibrational, electronic, and biological aspects of ANGA. The FTIR and Raman spectral analyses have identified a number of functional groups. The stretching wave variety of the hydrogen bond acceptor O-H and donor COOH is shifted by the contact, as proven by the vibrational analysis. The grown crystal is a good candidate because of its broad range of transparency in the visible and ultraviolet regions. The stability and bioactivity of the molecule are shown by the HOMO–LUMO energy gap. Antibacterial evaluation can be used as a treatment for bacteria.

REFERENCES

[1] 4-Amino-2-bromopyridine CAS:7598-35-8 - A Versatile Chemical Building Block | 3,4-Dibenzyloxybenzaldehyde: A Versatile Chemical Compound with a Wide Range of Applications , Ningbo Inno Pharmchem Co.,Ltd.
[2] Priyashree Sindhu et al/ study of biological activities of thiourea and glutaric acid based template mediated complexes doped with metal (ii) sulphates, NeuroQuantology | September 2022| Volume 20 | Issue 11 | Page 8542-8551 |
[3] Glutaric Acid 2024. Dictionary of Toxicology, pp 426–427
[4] M.J. Frisch, G.W. Trucks, H.B. Schlegel, G.E. Scuseria, M.A. Robb, J.R. Cheese- man, G. Scalmani, V. Barone, B. Mennucci, G.A. Petersson, H. Nakatsuji, M. Caricato, X. Li, H.P. Hratchian, A.F. Izmaylov, J. Bloino, G. Zheng, J.L. Sonnen- berg, M. Hada, M. Ehara, K. Toyota, R. Fukuda, J. Hasegawa, M. Ishida, T. Naka- jima, Y. Honda, O. Kitao, H. Nakai, T. Vreven, J.A. Montgomery Jr., J.E. Peralta, F. Ogliaro, M. Bearpark, J.J. Heyd, E. Brothers, K.N. Kudin, V.N. Staroverov, T. Keith, R. Kobayashi, J. Normand, K. Raghavachari, A. Rendell, J.C. Burant, S.S. Iyengar, J. Tomasi, M. Cossi, N. Rega, J.M. Millam, M. Klene, J.E. Knox, J.B. Cross, V. Bakken, C. Adamo, J. Jaramillo, R. Gomperts, R.E. Stratmann, O. Yazyev, A.J. Austin, R. Cammi, C. Pomelli, J.W. Ochterski, R.L. Martin, K. Morokuma, V.G. Zakrzewski, G.A. Voth, P. Salvador, J.J. Dannenberg, S. Dapprich, A.D. Daniels, O. Farkas, J.B. Foresman, J.V. Ortiz, J. Cioslowski, D.J. Fox, Gaussian 09, Revision C.02,Gaussian Inc., Wallingford CT, 2010.
[5] O'Boyle NM, Tenderholt AL, Langner KM (2008) Cclib: a library for package-independent computational chemistry algorithms. J Comput Chem 29:839–845
[6] T. Lu, F. Chen, Multiwfn: a multifunctional wave function analyser, J. Comput. Chem. 33 (2012) 580–592, doi: 10.1002/jcc.22885 . 0000
[7] W. Humphrey, A. Dalke, K. Schulten, VMD: visual molecular dynamics, J. Mol. Graph. 14 (1996) 33–38, doi: 10.1016/0263-7855(96)0 0 018-5.
[8] T.Joselin Beaula, D. Manimaran, I. Hubert Joe, V.K. Rastogi, and V. Bena Jothy, "Vibrational Spectroscopic Studies and DFT Computation of the Nonlinear Optical Molecule L-Valinium Formate," Spectrochimica Acta. Part A, Molecular and Biomolecular Spectroscopy 126 (2014): 170–7. https://doi.org/10.1016/j.saa.2014.01.088.
[9] T. Joselin Beaula, A. Packiavathi, D. Manimaran, I. Hubert Joe, V.K. Rastogi, V. Bena Jothy, Quantum chemical computations, vibrational spectroscopic analysis and antimicrobial studies of 2,3-Pyrazinedicarboxylic acid, Spectrochimica Acta Part A: Molecular and Biomolecular Spectroscopy, Volume 138, 2015, Pages 723-735,
[10] S.M. Hiremath, A. Suvitha, N.R. Patil, C.S. Hiremath, S.S. Khemalapure, S.K. Pat- tanayak, V.S. Negalurmath, K. Obelannavar, Molecular structure, vibrational spectra, NMR, UV, NBO, NLO, HOMO-LUMO and molecular docking of 2-(4, 6- dimethyl-1-benzofuran-3-yl) acetic acid (2DBAA): experimental and theoreti- cal approach, J. Mol. Struct. 1171 (2018) 362–374, doi: 10.1016/j.molstruc.2018. 05.109.
[11] R.M. Silverstein , G.C. Bassler , T.C. Morril , Spectrometric Identification of Or- ganic Compounds, 5th ed., John Wiley and Sons, Inc., Singapore, 1991.
[12] B.C. Smith , Infrared Spectral Interpretation: A Systematic Approach, CRC Press, 1998 .
[13] P. Tarte, Infra-red spectra of inorganic aluminates and characteristic vibrational frequencies of AlO4 tetrahedra and AlO6 octahedra, Spectrochimica Acta Part A: Molecular Spectroscopy, Volume 23, Issue 7, 1967, Pages 2127-2143,
[14] C. Dabora Vincy, J.D. Deephlin Tarika, X.D. Divya Dexlin, A. Rathika, T. Joselin Beaula, Exploring the antibacterial activity of 1, 2 diaminoethane hexanedionic acid by spectroscopic, electronic, ELF, LOL, RDG analysis and molecular docking studies using DFT method, Journal of Molecular Structure, Volume 1247, 2022, 131388,
[15] Laurent Vannay,Benjamin Meyer, Riccardo Petraglia, Giuseppe Sforazzini, Michele Ceriotti and Clémence Corminboeuf, Analyzing Fluxional Molecules using DORI, Journal of Chemical Theory and Computation, copyright (C) American Chemical Society after peer review and technical editing by the publisher. To access the final edited and published work see https://pubs.acs.org/doi/10.1021/acs.jctc.7b01176